RESEARCH ARTICLE | DECEMBER 09 2024

Numerical study of wake flow across two circular cylinders in tandem arrangement with high rotation speed

Muhammad Aneeb Siddiqui ; Adnan Munir ; Muhammad Hamza Ali ; Ming Zhao ; Penghao Duan ; Muhammad Nafees Mumtaz Qadri

Physics of Fluids 36, 123613 (2024)
https://doi.org/10.1063/5.0242939

Physics of Fluids ARTICLE pubs.aip.org/aip/pof

Numerical study of wake flow across two circular cylinders in tandem arrangement with high rotation speed

Cite as: Phys. Fluids **36**, 123613 (2024); doi: 10.1063/5.0242939
Submitted: 8 October 2024 · Accepted: 16 November 2024 ·
Published Online: 9 December 2024

Muhammad Aneeb Siddiqui,[1,2] Adnan Munir,[1,3] Muhammad Hamza Ali,[1] Ming Zhao,[3,a)] Penghao Duan,[2,a)] and Muhammad Nafees Mumtaz Qadri[1]

AFFILIATIONS

[1]School of Mechanical and Manufacturing Engineering, National University of Sciences and Technology, H-12 Islamabad, Pakistan
[2]Department of Mechanical Engineering, City University of Hong Kong, Hong Kong
[3]School of Engineering, Design and Built Environment, Western Sydney University, Penrith, 2751 NSW, Australia

[a)]**Authors to whom correspondence should be addressed:** m.zhao@westernsydney.edu.au and pengduan@cityu.edu.hk

ABSTRACT

Flow behind a bluff body is marked with unstable wake pattern eventually impacting the forces acting on the body, which can be actively controlled by rotation. When multiple rotating bluff bodies are placed in close proximity, the wake flow and resulting forces are significantly affected by the mutual flow interaction, necessitating detailed analysis for practical applications. In this vein, this study investigates the variation in wake flow across two circular cylinders, placed in a tandem arrangement, for both co-rotation and counter-rotation configurations. Two-dimensional numerical simulations are performed at a low Reynolds number of 100 for three gap ratios of $L/D = 1.5$, 2, and 4, where L and D are the center-to-center distance between the cylinders and the cylinder diameter, respectively. The non-dimensional rotation rate is varied from 0 to 6 for the co-rotation configuration and the range is extended till 15 for counter-rotation configuration to capture the secondary instability regime of the system. Flow regimes and force coefficients are analyzed to qualitatively and quantitatively map the overall system behavior, respectively. The flow regimes observed for different rotation rates and L/D are noticed to be different combinations of the flow regimes observed for a single rotating cylinder. Irrespective of the co-rotation or counter-rotation configuration, the dominant frequency of secondary vortex shedding for both upstream and downstream cylinder is noticed to be same, indicating that either a single vortex is shed from the system or a synchronized vortex pair is shed with one vortex from each cylinder. Compared to the co-rotating cylinders, counter-rotating cylinders demonstrate predominant inclination toward steady flow behavior over majority of the studied rotation rates.

I. INTRODUCTION

Study of flow around bluff bodies, specifically cylinders, has been of paramount importance as it not only provides clarity about different flow properties but also forms the basis for flow field studies around other complex geometries. The shedding of vortices induces instability in the flow, eventually resulting in application of fluctuating forces on bluff bodies. These forces are of great interest in engineering applications as they can cause structural failure owing to resonance and they promote multiple fluid phenomena, including noise sources and instability. Vortices shedding from bluff bodies can be controlled in several ways, including creation of thermal non-homogeneity between the moving fluid and the bluff body, use of nanofluids, use of control cylinders, use of a small cylinder in the vicinity of a cylinder (control rod phenomena), and rotation of cylinder/cylinders. The present study employs the method of rotation to study the variation in vortex shedding across bluff bodies, which is important to understand for various practical applications. For high Reynolds number, such flows find their importance in modern Flettner rotors, where direct control of flow around circular cylinders is used in modern Flettner rotors to provide auxiliary propulsion thrust and economize fuel consumption (De Marco *et al.*, 2016). Some past studies have been dedicated to study the performance of Flettner rotors (Li *et al.*, 2024; Seddiek and Ammar, 2021), considering the impact of various flow parameters including flow speed and direction to enhance energy harnessing, Flettner spin ratio, rotor aspect ratio, and Flettner end plate dimension. Study of such flows at low Reynolds number is also crucial for the

understanding of convective transport phenomena including fluidized bed combustion, in particular pulverized coal combustion (Chatterjee and Chaitanya, 2020; Wu, 2005) where rotating cylinders create a zone in their proximity which acts as a buffer to the convective transport (Zhang *et al.*, 2024).

Vortex shedding across a cylinder generically initiates in the form of Von Karman vortices when the Reynolds number exceeds its critical threshold value of 45–50 (Pal Singh Bhinder *et al.*, 2012). Here, Reynolds number is defined as the ratio of inertial to viscous forces, formulated as $Re = \rho U_\infty / D$ with ρ, U_∞, and D being the density of fluid, freestream flow velocity, and diameter of the cylinder. It is noticed that introduction of more than one bluff bodies modifies the vortical pattern compared to a single bluff body (Meneghini *et al.*, 2001; Zdravkovich, 1977). Multiple experimental studies on different arrangements of circular cylinders are done by various authors including Kiya *et al.* (1993), Kiya *et al.* (1980), Meneghini *et al.* (2001) and Zdravkovich (1977, 1987). All these studies are aimed to better comprehend the fluid flow around different arrangements of bluff bodies. In the study of fluctuating and time averaged fluid forces acting on a system of two tandem circular cylinders (Moriya *et al.*, 2001), authors observed that the fluctuating lift and drag forces acting on the downstream cylinder were larger than the upstream cylinder. They also found clear relation between the fluctuating fluid forces on the downstream cylinder and the reattachment position of the shear layers. For small gap ratios of $L/D = 1.5$ and 2, where L is the center-to-center distance between the cylinders, negative drag is observed for downstream cylinder (Mittal *et al.*, 1997), which is reasoned due to the reattachment of shear layers from the upstream cylinder at the trailing region of downstream cylinder, providing a forward push, i.e., negative drag. Due to the same reason, the overall drag of the system of two cylinders is observed to be less than the drag of an isolated cylinder. A stabilizing effect is noticed from the downstream cylinder under the specific condition of L/D lower than drag inversion L/D (Carmo *et al.*, 2010).

As the knowledge of flow fields for stationary cylinders cannot be directly extrapolated to rotating cylinders due to involved flow complexities, separate analysis is required for predicting the corresponding flow patterns. Many numerical and experimental studies in the past have been dedicated to the investigation of the effect of rotation across single and multiple cylinders (Ali *et al.*, 2023; Behara *et al.*, 2022; Ansari *et al.*, 2024; Bhattacharyya *et al.*, 2022, 2023; Chatterjee and Chaitanya, 2020; Darvishyadegari and Hassanzadeh, 2019; Khan *et al.*, 2023, Krishna Chaitanya and Chatterjee, 2021; and Rastan *et al.*, 2021). With the application of angular rotations to circular cylinders, the local conditions favoring generation of vortices are compromised, eventually decreasing the vortex shedding frequency (Kumar *et al.*, 2011), leading to a stable flow field (Díaz *et al.*, 1983). Larger force coefficients are experienced by cylinders at higher rotation rates, due to the enhanced magnus effect; however, the power required to rotate the cylinder is also increased (Mittal and Kumar, 2003). For a single cylinder at low values of the non-dimensional rotation rate, typically less than $\alpha \approx 1.8$–1.9 for $Re = 100$ and 200, alternate vortex shedding, also known as primary vortex shedding, is observed from the cylinder. Here, the non-dimensional rotation rate α is defined as $\omega D / 2U_\infty$ where ω is the rotational speed of the surface of the cylinder. As α is increased beyond the primary vortex shedding regime, the flow become steady with no vortex shedding. For higher α values in the range of $4.8 \leq \alpha \leq 5.15$ at $Re = 100$ (Stojković *et al.*, 2002) and $4.34 \leq \alpha \leq 4.8$ at $Re = 200$ (Mittal and Kumar, 2003), unsteady periodic vortex shedding re-appears, however, with very less shedding frequency in comparison to the primary vortical shedding at lower α values. Such vortex shedding is termed as the secondary instability regime. Beyond the upper α boundary of this regime, the flow becomes steady again.

For a tandem arrangement of circular cylinders at a Reynolds number of 100, the rotation rates of $0 \leq \alpha \leq 2.75$ for different L/D were examined by Chatterjee *et al.* (2017) who found a significant dependence of the critical rotation rate on the gap ratio, for suppression of the primary vortex shedding. The positional variation of frontal stagnation points for $0 \leq \alpha \leq 4$ has been traced for 2D arrangement of tandem circular cylinders at a Reynolds number of 200 for $L/D = 1.5$, 2, and 4 (Darvishyadegari and Hassanzadeh, 2019). Dehkordi *et al.* (2011) studied the impact of laminar and turbulent flow conditions on two tandem cylinders, showing enhanced unstable behavior at higher Reynolds number owing to higher lift force fluctuations. For an isolated flow regime under specific flow conditions, it is noticed that in addition to the Reynolds number and inlet turbulence intensity, flow parameters are also dependent on cylinders' surface roughness (Dubois and Andrianne, 2022). Different authors have noticed differences in wake patterns due to the impact of cylinders' orientation in the overall arrangement (Hosseini *et al.*, 2021; da Silva and de Lima, 2020). Alam (2016) studied the effect of L/D and phase lag on the lift profile and Strouhal number and constructed an equation, concluding that the phase lag is a non-linear function of L/D, Strouhal number, and convection velocity of the vortices in a system of two circular cylinders placed in a tandem arrangement.

Flow fields obtained with the application of angular rotation to circular cylinders show prominent impact of rotation orientation, i.e., co-rotation and counter-rotation, on the overall vortex shedding pattern (Chan and Jameson, 2010; Chan *et al.*, 2011; Rastan *et al.*, 2021; and Yoon *et al.*, 2007), with the generic trend of enhanced flow field stability in the counter-rotation configuration as compared to the co-rotation configuration. Ansari *et al.* (2024) studied fluid flow for the co-rotation and counter-rotation configurations of two circular cylinders in multiple arrangements at a Reynolds number of 200 for $1.5 \leq L/D \leq 4$ and $0 \leq \alpha \leq 5$. They found that the critical rotation rates for co-rotating cylinders were 20% more than the counter-rotating cylinders in different arrangements. Yoon *et al.* (2007) studied two counter-rotating cylinders in a side-by-side arrangement and traced the critical α value for the flow transition from the primary vortex shedding regime to steady state regime.

From all the above studies, it is inferred that the effect of rotation of cylinders in tandem and side-by-side arrangement is investigated in detail, but majority of the works are limited to low α values, focusing on the primary stability (first steady state) of the overall system. However, the author highlights the importance to have cylinders system response documented at higher α values, especially in the secondary instability of the system to aptly refer the research outcomes in real life environments. Thus, to fill this knowledge gap, the present study is aimed at the numerical investigation of flow across two co-/counter-rotating cylinders placed in a tandem arrangement at high rotation rates. All the numerical simulations are performed at $R = 100$ for $L/D = 1.5$, 2, and 4, and α is increased till the value where secondary instability subsides. The outline of the rest of this paper is as follows.

The computation model and the governing equations are provided in Sec. II whereas the mesh sensitivity study and validation of the method are presented in the Appendix. Different flow regimes along with their mutual transitioning are discussed in Sec. III A and quantitative analyses of force coefficients are provided in Sec. III B. Eventually, Sec. IV presents the conclusive remarks.

II. NUMERICAL MODEL

Figure 1 shows the computational domain for simulating flow past two tandem circular cylinders. The center-to-center distance between the two cylinders is L, and D is the cylinder diameter. A non-dimensional rotation rate defined as $\alpha = \omega D/2U_\infty$ is applied to both cylinders, where U_∞ denotes the freestream flow velocity. The upstream and downstream cylinders are referred to as C1 and C2, respectively.

The Reynolds number is defined as $Re = \rho U_\infty D/\mu$ where ρ and μ, respectively, are the density and the dynamic viscosity of the fluid. The Cartesian coordinates x and y, time t, pressure p, and streamwise and transverse velocities u and v are non-dimensionalized as follows: $X = x/D$, $Y = y/D$, $T = tU_\infty/D$, $P = p/\rho U_\infty^2$, $U = u/U_\infty$ and $V = v/U_\infty$, respectively. The non-dimensional incompressible Navier–Stokes (N–S) equations, presented below, are the governing equations for simulating the flow,

$$\frac{\partial U}{\partial X} + \frac{\partial V}{\partial Y} = 0, \tag{2.1}$$

$$\frac{\partial U}{\partial T} + U\frac{\partial U}{\partial X} + V\frac{\partial U}{\partial Y} = -\frac{\partial P}{\partial X} + \frac{1}{Re}\left(\frac{\partial^2 U}{\partial X^2} + \frac{\partial^2 U}{\partial Y^2}\right), \tag{2.2}$$

$$\frac{\partial V}{\partial T} + U\frac{\partial V}{\partial X} + V\frac{\partial V}{\partial Y} = -\frac{\partial P}{\partial Y} + \frac{1}{Re}\left(\frac{\partial^2 V}{\partial X^2} + \frac{\partial^2 V}{\partial Y^2}\right). \tag{2.3}$$

Finite volume solver provided in ANSYS Fluent 18.2 is used to perform the numerical simulations using a structured mesh. The N–S equations are solved using Semi-Implicit Method for Pressure Linked Equations (SIMPLE) algorithm. A second order upwind scheme is used to perform the spatial discretization of convection and diffusion terms of the N–S equation. For spatial discretization of the pressure terms, a second order scheme is employed, and temporal discretization is achieved through an implicit second order scheme. The boundary conditions to solve the N–S equations are as follows. A uniform velocity is applied at the inlet boundary with streamwise and transverse components as $U = 1$ and $V = 0$, respectively. Top and bottom boundary domains are defined as symmetry, whereas the velocity gradients and the pressure value are set to zero for the outlet boundary. A no-slip boundary condition is used for cylinders' surfaces, which means that the surface velocity is the same as the rotational speed. The solution convergence criterion for residual values is set to 10^{-6} and a non-dimensional time step of 0.001 is used for all the simulations. Mesh sensitivity study and numerical validation were conducted to ensure the accuracy of solutions (see the Appendix).

The pressure and shear stresses are integrated over the surface of each cylinder to calculate its lift and drag force, F_L and F_D, respectively. These forces are normalized to get the lift and drag coefficients as $C_L = 2F_L/\rho U_\infty^2 D$ and $C_D = 2F_D/\rho U_\infty^2 D$, respectively. The mean force coefficients $\overline{C_{Lk}}$ and $\overline{C_{Dk}}$, where $k = 1$ or 2 represents the cylinder C1 or C2, respectively, are calculated by averaging the lift and drag coefficients over a minimum of 5 vortex shedding periods when the system has periodic vortex shedding. The standard derivation of the drag and lift coefficients of the k th cylinder are defined as C'_{Dk} and C'_{Lk}, respectively. The vortex shedding frequency is obtained by analyzing the time history of the lift coefficients using fast Fourier transform (FFT). The peak frequency f of a FFT spectrum is the vortex shedding frequency, and the Strouhal number is correspondingly defined as $St = fD/U_\infty$.

III. RESULTS AND DISCUSSION

Two-dimensional numerical simulations are conducted at a Reynolds number of 100 and gap ratios $L/D = 1.5$, 2, and 4. Munir *et al.* (2019) investigated the flow past a rotating cylinder at high

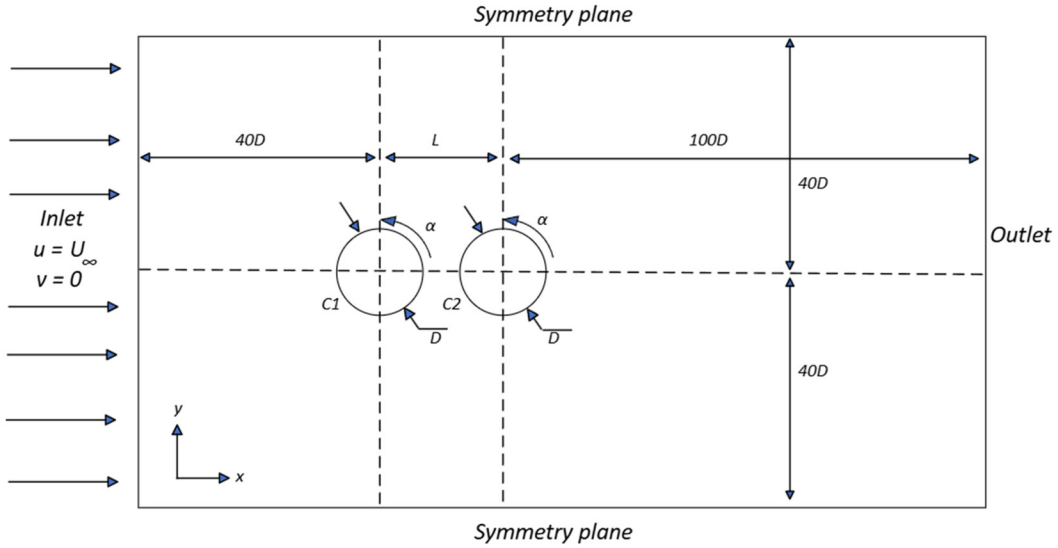

FIG. 1. Schematic diagram for computational domain (not to scale).

rotation rate and found that the flow is two-dimensional at Reynolds number for rotation rates up to 250, thus a Reynolds number of 100 is chosen for the present study. The analysis is done for two configurations of angular rotations: co-rotation configuration where both the cylinders rotate in the anticlockwise direction and counter-rotation configuration where C1 and C2 rotate in anticlockwise and clockwise directions, respectively. The non-dimensional angular rotation ranges from $\alpha = 0$ to a value where further increase in angular rotation does not yield any change in the flow pattern. The maximum value of α for the co-rotation configuration is 6 whereas for the counter-rotation configuration, the maximum value of 15 is considered. The vortex shedding patterns for all the cases are analyzed to identify various regimes. The prime focus is laid on the secondary instability of the wake which causes significant enhancement of vortex shedding and increase in the force coefficients. Refined simulations with smaller intervals of α are conducted to accurately identify the starting and ending rotation rates of the secondary instability regimes.

A. Flow regimes

1. Flow regimes for a single cylinder

The flow past a single rotating cylinder, simulated for $\alpha = 1$–6 with a gap of 1 in our previous study (Ali *et al.*, 2023), was first analyzed and the identified wake patterns are found to agree with those reported in previous studies of a single cylinder (Lu *et al.*, 2011; Mittal and Kumar, 2003; Munir *et al.*, 2019; Stojković *et al.*, 2002; and Yang *et al.*, 2023). Based on the vortex shedding pattern, the wakes are classified into five regimes as shown in Figs. 2(a)–2(e).

1. The vortex shedding (VS) regime, also referred to as primary instable flow, is observed at low α values. In the VS regime,

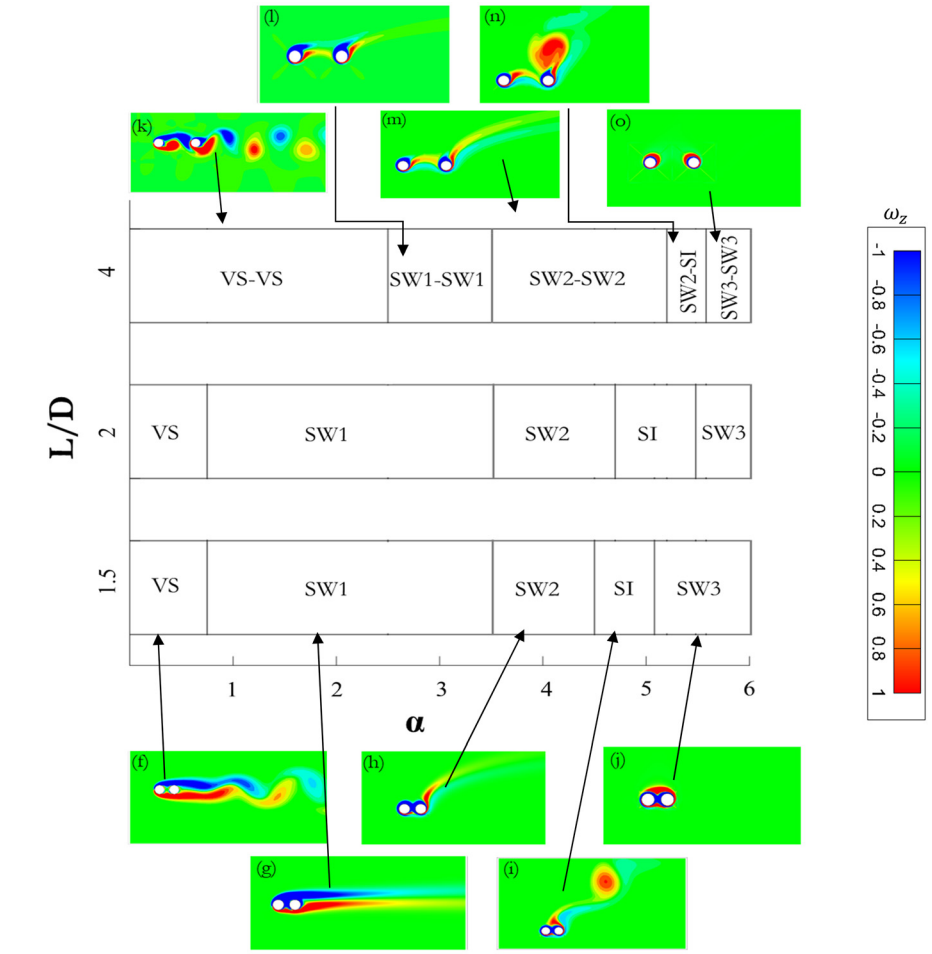

FIG. 2. Flow regimes map and vorticity contours for co-rotating tandem cylinders over L/D vs α spectrum.

Flow regimes and vorticity contours for tandem corotating cylinders

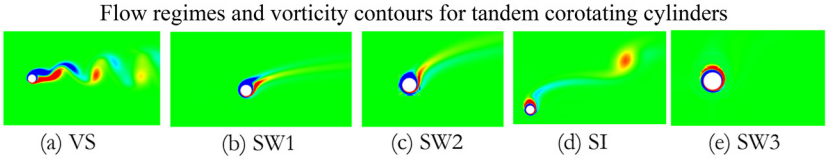

(a) VS (b) SW1 (c) SW2 (d) SI (e) SW3

Vorticity flow contours for rotating single cylinder

positive and negative vortices are shed from the two sides of the cylinder in a periodic manner [Fig. 2(a)], and the flow is asymmetric when rotation is non-zero.
2. In the steady wake 1 (SW1) regime, two shear layers are separated from two sides of the cylinder, and they do not form vortex shedding [Fig. 2(b)].
3. In the steady wake 2 (SW2) regime, the effect of α is considerable enough that one shear layer goes around the cylinder and sheds from the same side as another shear layer, thus both shear layers are separated from the cylinder from the same side, forming two elongated shear layers [Fig. 2(c)].
4. In the secondary instability (SI) regime, shear layers first wrap around the cylinder and then stretch, ultimately forming large vortices that are periodically shed from the cylinder wake [Fig. 2(d)]. The vortex shedding period of this regime is much longer than that of the VS regime.
5. In the steady wake 3 (SW3) regime, the wake transitions back into a stable state in which shear layers wrap around the cylinder [Fig. 2(e)].

2. Flow regimes for two co-rotating cylinders

All the five regimes observed in the case of single cylinder was also observed in the case of two tandem cylinders. When the two cylinders are sufficiently separated from each other, there is a separate wake behind each cylinder. In this case, the wake regime name is in the format of name1-name2, where name1 and name 2 are the regime names of C1 and C2, respectively, and they may be different in some cases. For example, the wake name SW2–SI means the wake of C1 is SW2 and the wake of C2 is SI. When the two cylinders are very close to each other, they behave like a single body and there is only one wake. For example, the wake name SW2 means that the two cylinders behave as one body with a combined SW2 wake. All the identified wake regimes are given in Fig. 2. The wake patterns for $L/D = 1.5$ and 4 are shown in the figure whereas the wake patterns for $L/D = 2$ are not presented as they are the same as those for $L/D = 1.5$.

a. L/D = 1.5 and 2. For $L/D = 1.5$ and 2, the rotation speeds of the surfaces of the two cylinders in the gap are in opposite directions to each other; as a result, the velocity in the gap is weak. The two cylinders behave as a single body with only one wake for the simulated range of rotation rate. At low α values ($0 \leq \alpha \leq 0.75$), the shear layers from C1 reattach to C2, then the combined shear layers separate from C2, forming a single periodic wake pattern in the VS regime as seen in Fig. 2(f). For $0.75 \leq \alpha \leq 3.5$, primary stable flow regime SW1 is observed for both $L/D = 1.5$ and 2, where the flow is steady and does not show any dynamic vortex shedding [Fig. 2(g)]. Further increase in the rotation rate results in the regime SW2 as shown in Fig. 2(h), where two shear layers are separated from the bottom side of C2. The regime SI, shown for $L/D = 1.5$ in Fig. 2(i), is very similar to the one for a single cylinder case shown in Fig. 2(d), only with stronger wake vortices. When the rotation rate exceeds the upper α boundary of the regime SI, the wake become steady again and the regime is SW3 [Fig. 2(j)].

The evolution of the dynamic wake in the regime SI within one vortex shedding period for $L/D = 1.5$ and 2 is shown in Fig. 3. A single vortex forms above both the cylinders in each vortex shedding period and its strength increases before it is shed from near C2.

In regime SI, the flow patterns for $L/D = 1.5$ and 2 are very similar to each other as can be seen in Fig. 3. For $L/D = 1.5$ and 2, SI flow regime starts and ends at α ranges of $4.5625 \leq \alpha \leq 5.175$ and $4.718\,75 \leq \alpha \leq 5.468\,75$, respectively. To study the impact of increasing α within the regime SI, three cases of $\alpha = 4.75$, 5, and 5.4375 are selected and discussed on the basis of time histories of the force coefficients and vortex shedding frequency. The force coefficients have a large mean value difference and only the oscillatory component of the force coefficients, $C_L - \overline{C}_L$ and $C_D - \overline{C}_D$, are shown in Fig. 4 for better comparison, along with the FFT spectra of the cases.

The oscillation of force coefficients is found to be periodic for all the simulated cases. The variation in time series data of force coefficients, presented in Figs. 4(a), 4(c), and 4(e) for $\alpha = 4.75$, 5, and 5.4375, respectively, indicate that with increase in α, the regime SI wake flow is modified, but the C_L for both C1 and C2 remains almost in-phase, whereas C_D shows anti-phase behavior for both C1 and C2. It is also noticed that C_L and C_D for C1 are mutually out-of-phase, whereas they are in-phase for C2. The amplitude and time period for both C_L and C_D of each cylinder exhibit a direct proportion with α, i.e., they increase with increase in α. Moreover, multiple frequencies of small amplitude are induced with increase in α as can be seen in the FFT spectra [Figs. 4(b), 4(d), and 4(e)]. Irrespective of α, the frequency

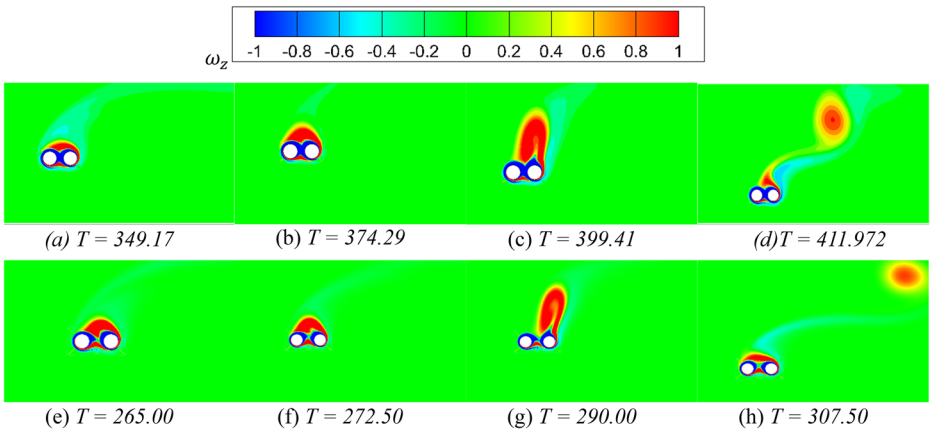

FIG. 3. Evolution of the wake within one vortex shedding period for regime SI for co-rotating cylinder at $\alpha = 5$: (a)–(d) $L/D = 1.5$; (e)–(h) $L/D = 2$.

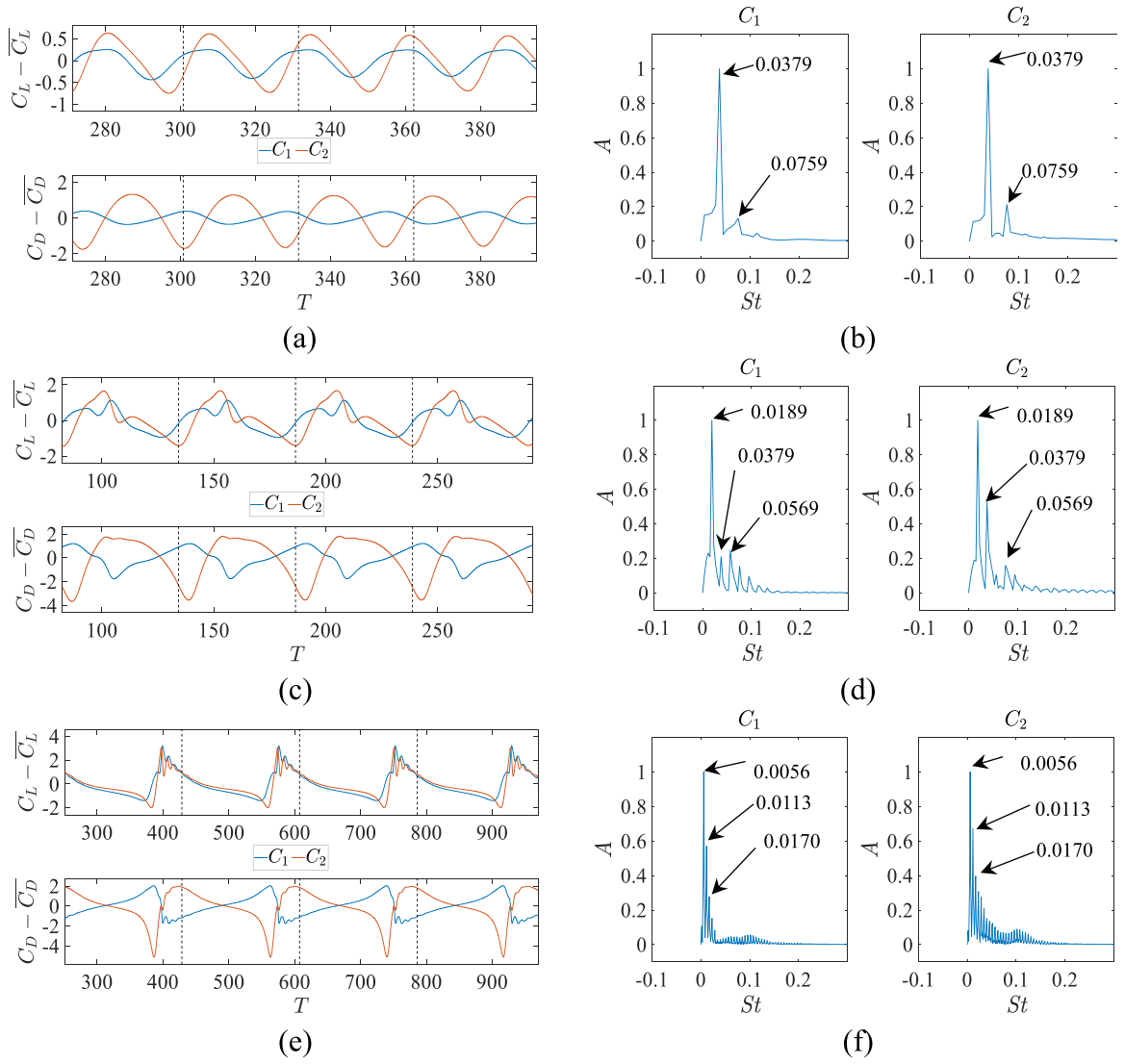

FIG. 4. Mean subtracted time histories of C_L and C_D for co-rotating cylinders at $L/D = 2$: (a) $\alpha = 4.75$ (c) $\alpha = 5$ (e) $\alpha = 5.4375$; frequency spectrum of lift coefficients: (b) $\alpha = 4.75$ (d) $\alpha = 5$ (f) $\alpha = 5.4375$.

modes for C1 and C2 remain identical, showing that the vortices are shedding from both the cylinders collectively. However, the frequency amplitude of C1 is comparatively larger than C2 because the variation of vorticity packet near C1 is relatively significant compared to C2, during each vortex shedding cycle. The dominant vortex shedding frequency, i.e., the one with the highest amplitude, varies with α such that for $\alpha = 4.75$, 5, and 5.4375, it transitions as 0.03, 0.01, and 0.005, respectively, indicating an increase in the vortex shedding period as α is increased. The other low amplitude modes in the frequency spectrum for higher α are also shrinking close to the dominant mode as deduced from the comparison of Figs. 4(b), 4(d), and 4(f).

b. L/D = 4. The gap of $L/D = 4$ has been sufficient to allow both cylinders to have their individual wakes. At small rotation rates of $0 \leq \alpha \leq 2.5$, the cylinders C1 and C2 shed vortices separately, and the wake is in regime VS–VS as seen in Fig. 2(k). Regime VS–VS was also termed as alternate co-shedding flow (AC) (Rastan *et al.*, 2021). As α is increased to lie in a range of $2.5 \leq \alpha \leq 3.5$, both C1 and C2 have their own separated shear layers, and the flow is in steady regime SW1–SW1 as shown in Fig. 2(l). Further increase in α within the range $3.5 \leq \alpha \leq 5.03$ makes the flow transition into regime SW2–SW2, where shear layers from each cylinder separate from one side of the corresponding cylinder, as can be seen in Fig. 2(m). As the rotation rate is in the range $5.03 \leq \alpha \leq 5.59$, the wake is in regime SW2–SI, where the wake of C2 changes to SI but the wake of C1 remains SW2. In this regime, the shear layers that are separated from C1 reattaches to C2 without vortex shedding, as shown in Fig. 2(n), while the SI wake of C2 is similar to that of a single cylinder. At $L/D = 4$, SI wake is not

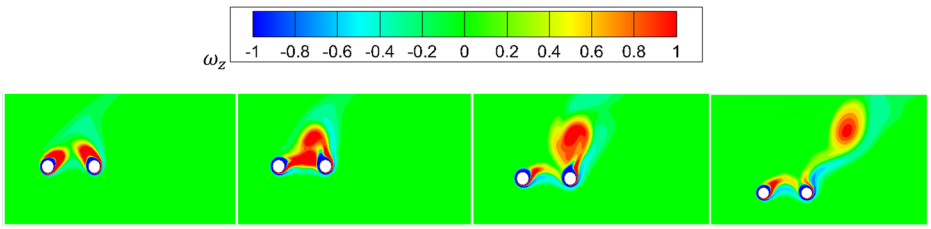

FIG. 5. Evolution of the wake within one vortex shedding period for regime SW2–SI for co-rotating cylinder at $L/D = 4$ and $\alpha = 5.25$.

found behind C1 over all the studied rotation rates. As the rotation rate increases to $\alpha = 5.59$ and beyond, the wakes of both C1 and C2 are SW3, forming a regime SW3–SW3 as shown in Fig. 2(o).

Figure 5 presents the time evolution of wake flow in the regime SW2–SI rotation configuration for $L/D = 4$ and $\alpha = 5.25$. At the beginning of the vortex shedding cycle, both cylinders have separate wake where the shear layers of each cylinder are wrapped around its surface, similar to a SW3–SW3 wake [Fig. 2(o)]. The positive vorticity packet around each cylinder grows stronger, however the presence of C2 stops the shear layers from C1 to roll up and form vortex shedding. The positive shear layer of C1 stretches in the gap and reattaches to the positive shear layer of C2, forming a SW2 wake pattern for C1 which is the same as previously observed for C1 in the regime SW2–SW2. The vorticity in the positive shear layer of C2 strengthens and eventually separates from the system. Thus, only one vortex is shed from C2 in one vortex shedding period whereas C1 retains the SW2 wake pattern. Although the wake at the beginning of a vortex shedding cycle appears like SW3–SW3, however, during the rest of the vortex shedding cycle [Figs. 5(b)–5(d)], the wake of C1 becomes SW2 and that of C2 becomes SI, as a result, the overall wake is defined as SW2–SI.

3. Flow regimes for two counter-rotating cylinders

Figure 6 presents the flow regime classification and wake flow patterns for the counter-rotation configuration of two tandem cylinders. When the two cylinders rotate in opposite directions, the surface velocity at the leeward side of C1 is in same direction as the surface velocity at the windward side of C2, resulting in a cross-flow velocity within the gap in the direction of the surface velocity. In the presently studied case, where C1 rotates in a counterclockwise direction whereas C2 rotates in a clockwise direction, the gap flow has significant upward cross-flow velocity and as a result, the flow direction relative to C1 is significantly deflected diagonally upward at high rotation rates as can be deduced from the vortex shedding patterns in Fig. 6. On the contrary, due to clockwise rotation, the wake of C2 deflects downward,

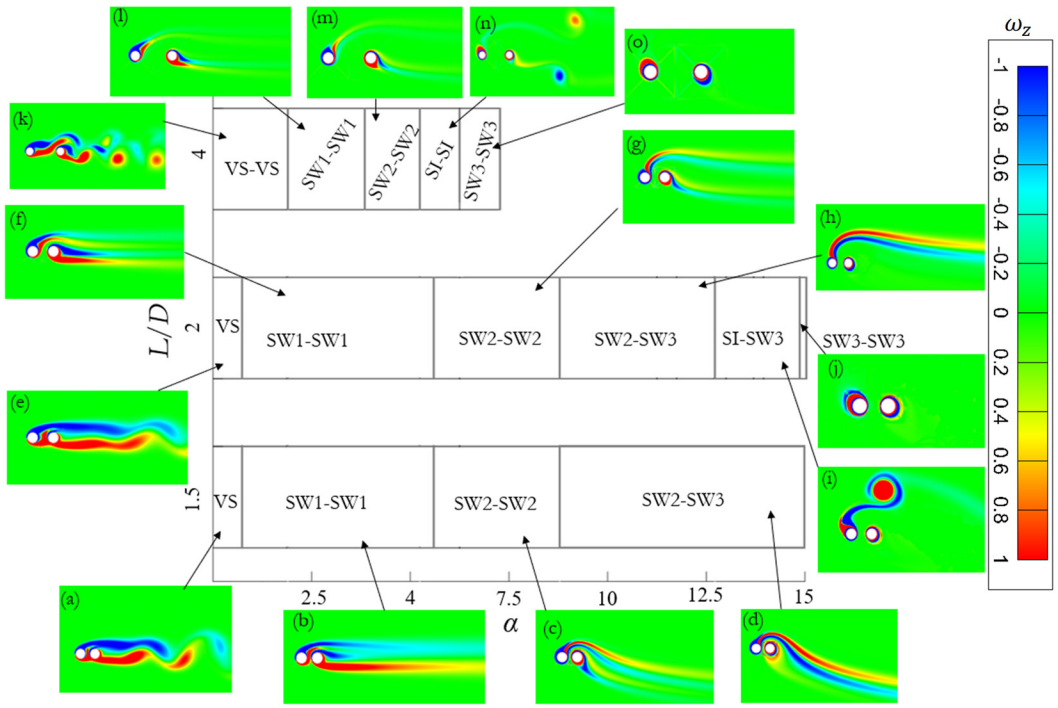

FIG. 6. Flow regimes map and vorticity contours for counter-rotating tandem cylinders over L/D and α spectrum.

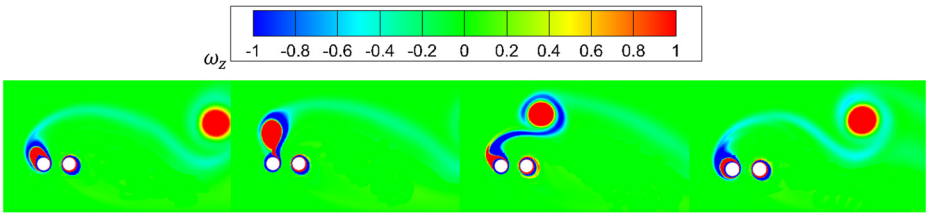

FIG. 7. Evolution of the wake within one vortex shedding period for regime SI–SW3 for counter-rotating cylinders at $L/D = 2$ at $\alpha = 12$.

although it is not as significant as in C1. The diagonal alignment of the wakes of C1 and C2 with opposite alignment angles avoids interaction between the wakes of C1 and C2 especially at higher α values, resulting in flow patterns with two distinct wakes, except when the rotation rate is very small.

a. L/D = *1.5 and 2.* At $L/D = 1.5$ and 2, the single body regime VS [Figs. 6(a) and 6(e), respectively] only occurs within a very narrow range of rotation rates $0 \leq \alpha \leq 0.75$. As α exceeds the value of 0.75, the flow has two wakes and the wake pattern of each wake changes with increase in α.

When $0.75 \leq \alpha \leq 4.5$ for both $L/D = 1.5$ and 2, the flow from each cylinder has a SW1 wake, forming the regime SW1–SW1 [Figs. 6(b) and 6(f), respectively]. The wake transitions to regime SW2–SW2 when the rotation rate is in the range of $4.5 \leq \alpha \leq 7.5$ for both the gap ratios [Figs. 6(g) and 6(e), respectively]. In both the regimes SW1–SW1 and SW2–SW2, the interaction between the two wakes from the cylinders is very weak because the enhanced upward cross-flow velocity in the gap prevents the shear layers of C1 from reattaching over C2. With increase in α beyond the upper boundary of $\alpha = 7.5$ for the regime SW–SW2 for both $L/D = 1.5$ and 2, the wake of C2 transitions to SW3 without going through SI, while the wake of C1 remains SW2, forming the regime SW2–SW3, as can be seen in Figs. 6(d) and 6(h). As α is further increased, the wake remains in the regime SW2–SW3 for $L/D = 1.5$ until the largest simulated $\alpha = 15$. On the other hand, for $L/D = 2$, while the wake of C2 does not change, the wake of C1 transitions to the SI wake as α is within the range of $11.25 \leq \alpha \leq 14.75$, resulting in a regime SI–SW3. Further increase in α beyond 15.74 results in the regime SW3–SW3 for $L/D = 2$.

The wake of C2 transitions to SW3 earlier than C1 because the shear layers from C2 at its bottom side are significantly attracted by the strong upward cross-flow velocity within the gap. As a result, the shear layers of C2 wrap around itself at smaller α than C1 and form SW3 wake. With further increase in α, the SW3 wake of C2 strengthens, preventing C2 from forming vortex shedding. Hence, the SI wake is not observed for C2.

Figure 7 shows one complete vortex shedding cycle in the regime SI–SW3 for the counter-rotation configuration at $L/D = 2$ and $\alpha = 12$. It can be seen that only one vortex is shed from C1 in a vortex shedding cycle whereas no vortex is shed from C2, and its shear layers are wrapped around its surface. The strong upward cross-flow velocity in the gap enhances the vortices that are generated from C1 but reduce the strength of the shear layers from C2, resulting in strong vortex shedding in SI mode from C1 and a SW3 wake for C2 with very weak shear layers wrapping around C2. The strength of the SI vortex from C1 in counter-rotation configuration (Fig. 7) is much stronger than the SI vortex from C2 observed in the SW2–SI regime for co-rotation configuration (Fig. 5). It is interesting to note that each positive vortex that is shed from C1 is enclosed within a weak negative vorticity packet originating from the negative shear layer of C1.

b. L/D = *4.* For counter-rotating cylinders at $L/D = 4$, periodic vortices are shed from both cylinders when α is in the range $0 \leq \alpha \leq 2$, and the flow regime is termed as regime VS–VS as can be seen in Fig. 6(k). The interaction between the two VS wakes is much weaker than that in the co-rotating case [Fig. 2(k)], because the VS wake of C1 biases toward the upward side avoiding interaction with C2. Because of the weak interaction between the wakes from C1 and C2, the wake patterns of each cylinder are very similar to that of a single cylinder, except that the wakes are deflected in opposite directions. Over the whole studied range of the rotation rates, the wakes of C1 and C2 remain isolated and are always in the same regime. With increase in α beyond the upper α boundary of the regime VS–VS, the wake goes through regime SW1–SW1 for $2 \leq \alpha \leq 3.5$, regime SW2–SW2 for $3.5 \leq \alpha \leq 5.37$, regime SI–SI for $5.37 \leq \alpha \leq 6.12$, and regime SW3–SW3 for $\alpha = 6.12$ or higher, as illustrated in Figs. 6(k)–6(o). The sequence of wake transition of each cylinder for the present configuration is the same as that of a single cylinder [Figs. 2(a)–2(e)].

Figure 8 presents one complete vortex shedding cycle in the regime SI–SI for the counter-rotation configuration at $L/D = 4$ and $\alpha = 5.5$. Since the vortices that are generated from the top right side of C1 and bottom right side of C2 move in two different diagonal

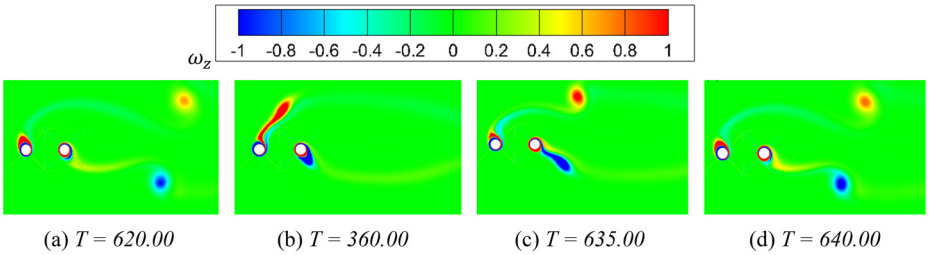

FIG. 8. Evolution of the wake within one vortex shedding period for regime SI–SI for counter-rotating cylinders at $L/D = 4$ and $\alpha = 5.5$.

directions due to opposite rotation, no vortex interaction occurs downstream. The vortex shedding pattern of each cylinder is similar to that of a single cylinder shown in Fig. 2(d).

B. Force statistics

1. Mean force coefficients

Figures 9(a)–9(c) present the variation of the mean lift and drag coefficients with α for the co-rotation configuration at $L/D = 1.5$, 2, and 4, respectively. As can be seen, the overall trend of the mean force coefficients is similar across the different gap ratios. Although, the overall wake flow regimes at $L/D = 4$ are different from those at $L/D = 1.5$ and 2, there is a generic similarity in the wake flow transition, causing the mean force coefficients to have a similar trend over α. Thus, further discussion on $L/D = 1.5$ also applies to $L/D = 2$ and 4. At $L/D = 1.5$ for the co-rotating configuration [Fig. 9(a)], it is observed that the magnitudes of both $\overline{C}_{L1}$ and $\overline{C}_{L2}$ increase with increase in α. Both $\overline{C}_{L1}$ and $\overline{C}_{L2}$ are in the negative direction because the two cylinders act as a single body and rotation is counterclockwise. In the co-rotation configuration, $\overline{C}_{D1}$ and $\overline{C}_{D2}$ are repulsive to each other, when the rotation rate is 2 or above, and their magnitude increases significantly with increase in α. The absolute magnitudes of

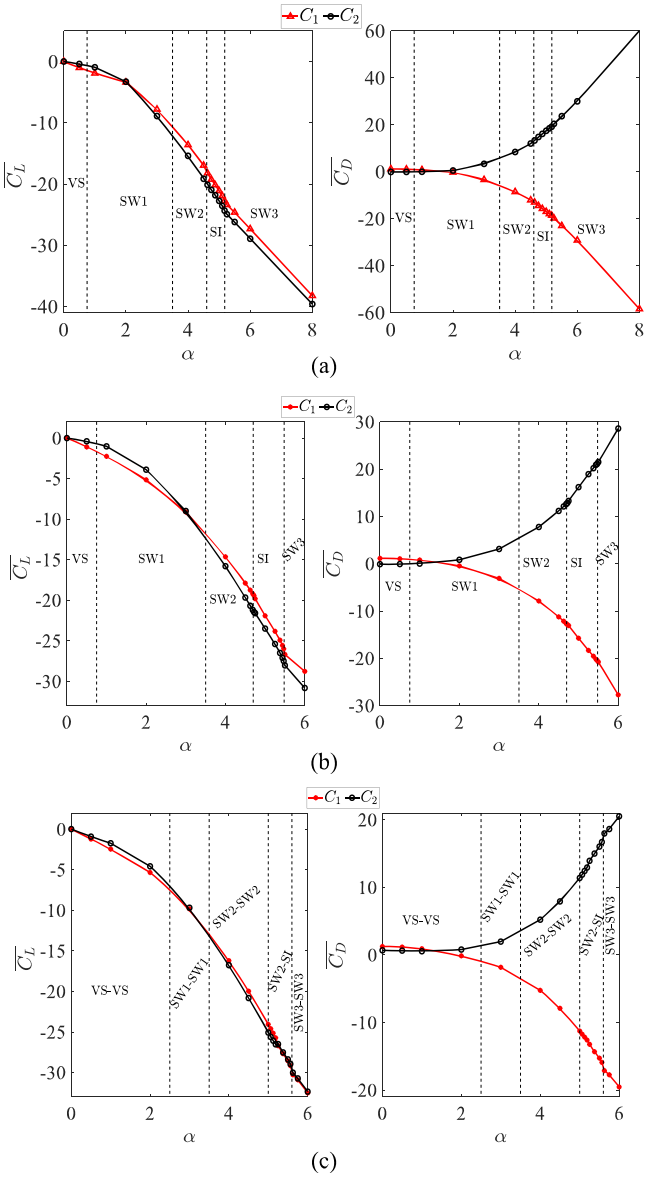

FIG. 9. Mean force coefficients for the co-rotation configuration at (a) $L/D = 1.5$; (b) $L/D = 2$; (c) $L/D = 4$.

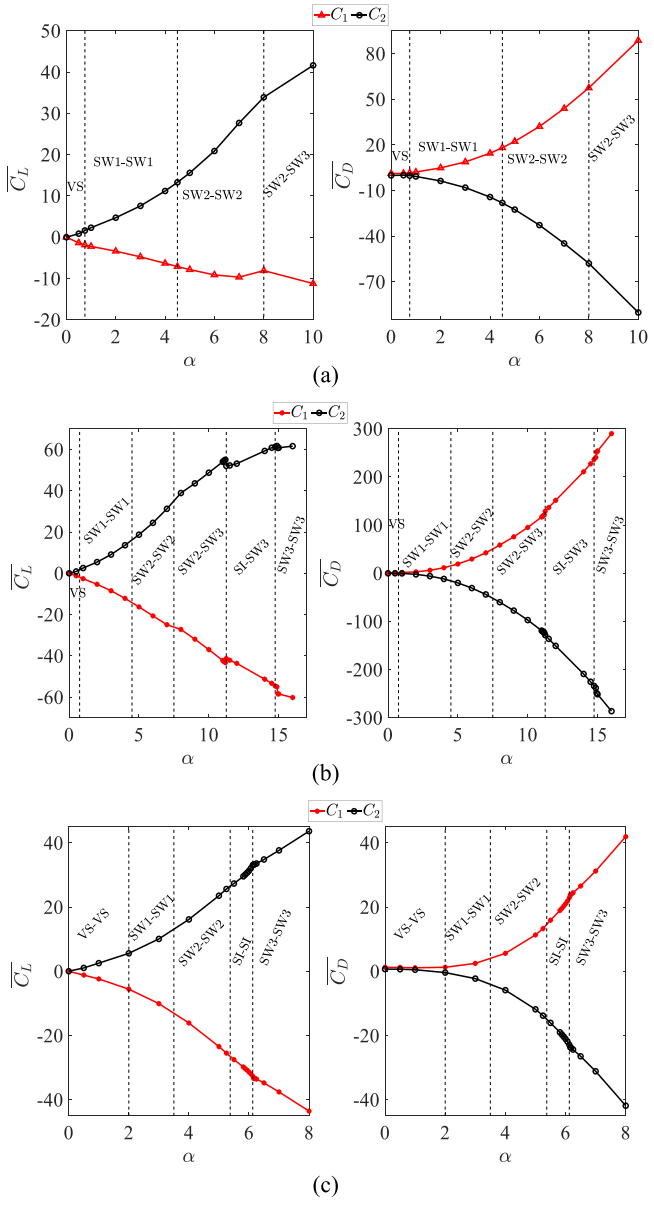

FIG. 10. Mean force coefficients for the counter-rotation configuration at (a) $L/D = 1.5$; (b) $L/D = 2$; $L/D = 4$.

$\overline{C}_{D1}$ and $\overline{C}_{D2}$ remain nearly equal where $\overline{C}_{D1}$ is negative and $\overline{C}_{D2}$ is positive. The reason for the negative drag for C1 in the co-rotation configuration is the increased gap pressure associated with the presence of stagnation point between the cylinders because of opposite rotational flow direction in the gap. The high stagnation pressure in the gap region causes repulsive drag forces to push both cylinders away from each other. With increase in the gap ratio, the gap stagnation pressure is lowered due to reduced interaction of the rotational flow and, therefore, a decrease in the repulsive gap force is observed. This results in a lower magnitude of $\overline{C}_{D1}$ and $\overline{C}_{D2}$ at a higher gap ratio for the corresponding α.

Figures 10(a)–10(c) present the variation in mean lift and drag coefficients with α for the counter-rotation configuration at $L/D = 1.5$, 2, and 4, respectively. The variation in mean force coefficients with increase in α has a generic similarity across all three gap ratios and the corresponding absolute magnitudes of the force coefficients for C1 are nearly equal to those of C2, except for the lift coefficients at $L/D = 1.5$ [Fig. 10(a)]. With increase in α for all three gap ratios, the magnitude of both $\overline{C}_{L1}$ and $\overline{C}_{L2}$ increases in the negative and positive directions, respectively, where the change is more significant for C2 as compared to C1 only at $L/D = 1.5$. This atypical variation at $L/D = 1.5$ in the counter-rotation configuration can be better explained by observing the position of stagnation points on each cylinder as illustrated in Fig. 11. The stagnation points for C1 and C2 in Fig. 11 are represented by points A and B, respectively. The less and more variation in the magnitude of $\overline{C}_{L1}$ and $\overline{C}_{L2}$, respectively, with increase in α can be justified by observing the high-pressure blobs at the stagnation points of both cylinders. With increase in α, the change in strength of the high-pressure blob at the stagnation point A of C1 is relatively very small as compared to the change at the stagnation point B of C2 as can be deduced by comparing the cases of $\alpha = 1$ and 5 presented in Fig. 12. Therefore, the pressure difference across C1 is less as compared to C2, resulting in a lower magnitude for the former and a higher magnitude for the latter. At each gap ratio, both $\overline{C}_{L1}$ and $\overline{C}_{L2}$ are in opposite directions as the rotating directions of C1 and C2 are opposite to each other. The variation in mean drag coefficients for both cylinders, $\overline{C}_{D1}$ and $\overline{C}_{D2}$, with increase in α is similar but opposite to that observed for the co-rotation configuration, i.e., $\overline{C}_{D1}$ is now positive and $\overline{C}_{D2}$ is negative, causing a strong attractive force between both cylinders.

2. Standard deviation of force coefficients

The standard deviation (SD) of the force coefficients for the co-rotation configuration of the two cylinders at $L/D = 1.5$, 2, and 4 is shown in Figs. 12(a)–12(c). The variations in SD force coefficients over α are similar for all the gap ratios, thus only the case of $L/D = 1.5$ is discussed further. In the regimes where the wake is steady, the SD of the force coefficients is zero. The variations of C'_{L1} and C'_{L2} with increase in the rotation rate follow a mutually similar trend in the VS regime, and so do C'_{D1} and C'_{D2}. The onset of the SI wake for the co-rotation configuration causes significant increase in SD of the lift and drag coefficients due to strong vortices in the wake (Fig. 3) compared to the VS regime [Fig. 2(f)]. In the SI regime for the co-rotation configuration, C'_{D1} is smaller than C'_{D2} because the shed vortices are closer to C2 than C1, when they are separated from the two cylinders system. For the gap ratio of $L/D = 4$ in the SI wake regime SW2–SI, although C1 has SW2 wake, the SD force coefficients of C1 are non-zero due to the dynamic SI wake of C2 and the shear layer interaction of C1 with C2 (Fig. 5).

For the counter-rotation configuration, the variation of SD force coefficients for $L/D = 1.5$, 2, and 4 is presented in Figs. 13(a)–13(c). For $L/D = 1.5$, the SD values are non-zero only in the regime VS since it is the only regime with vortex shedding. For $L/D = 2$ and 4, the SD values are non-zero in the regimes with VS and SI wakes. Compared to the regimes with VS wake observed at lower gap ratios for $L/D = 1.5$ and 2, the VS wake regime at $L/D = 4$ has significantly higher SD lift and drag coefficients where the SD values for C2 are higher than for C1. Same as observed for the co-rotation configuration, there is a significant increase in SD values as the SI wake flow develops, i.e., regime SI–SW2 at $L/D = 2$ and regime SI at $L/D = 4$. The SD values at $L/D = 2$ are significantly greater than the SD values at $L/D = 4$ since the SI wake vortex is very strong for the former case (Fig. 7) and comparatively weaker for the latter case (Fig. 8). Like the co-rotation configuration in the regime SW2–SI at $L/D = 4$, although C2 has a steady wake, the SD values of C2 are non-zero for the counter-rotation configuration in the regime SI–SW3 at $L/D = 2$.

3. Vortex shedding frequency

The time histories of the lift coefficients are analyzed in the frequency spectrum to identify the vortex shedding frequency normalized

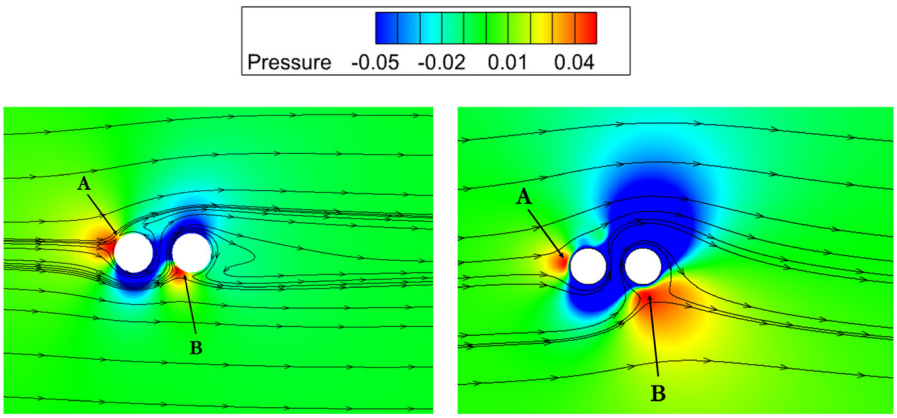

(a) $L/D = 1.5$: $\alpha = 1$ (b) $L/D = 1.5$: $\alpha = 5$

FIG. 11. Pressure contours and streamlines for the counter-rotation configuration at $L/D = 1.5$: (a) $\alpha = 1$; (b) $\alpha = 5$.

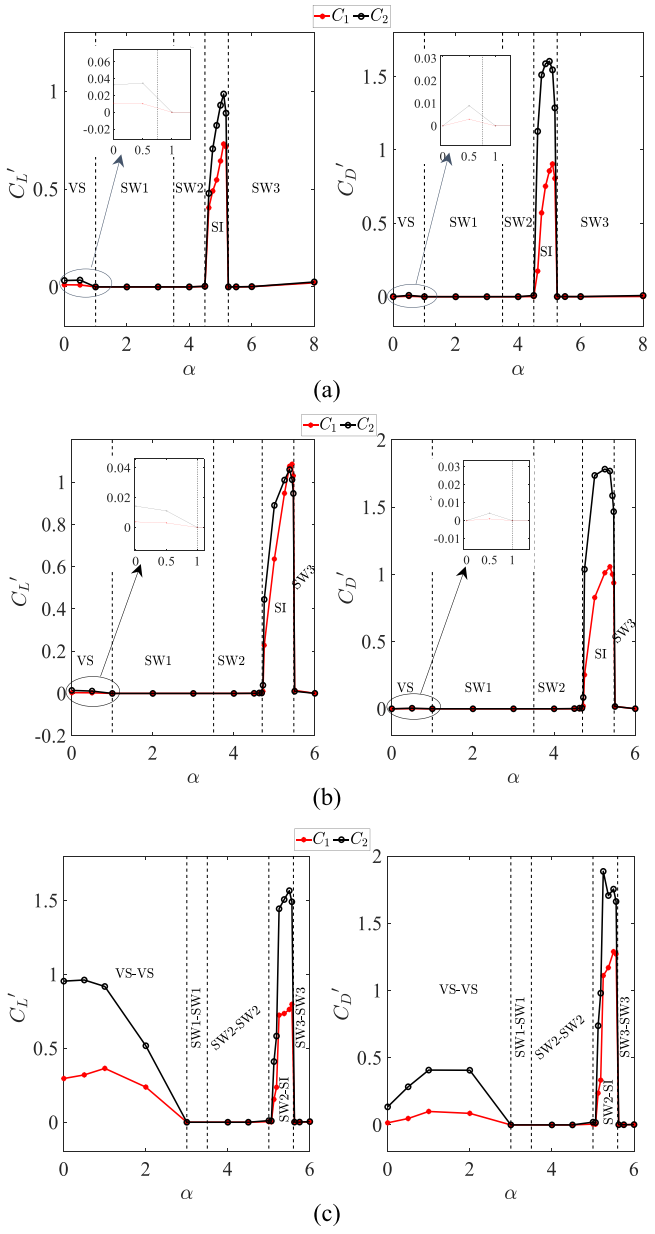

FIG. 12. Standard deviation of force coefficients for the co-rotation configuration at (a) $L/D = 1.5$; (b) $L/D = 2$; $L/D = 4$.

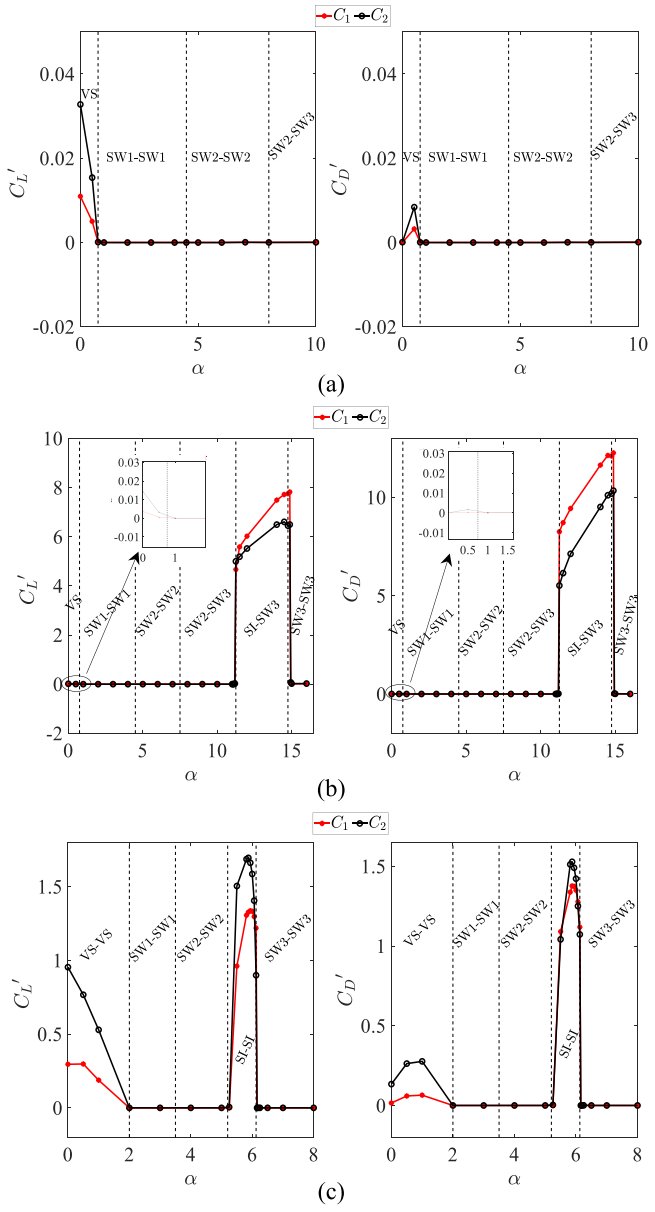

FIG. 13. Standard deviation of force coefficients for the counter-rotation configuration at (a) $L/D = 1.5$; (b) $L/D = 2$; $L/D = 4$.

as Strouhal number. For the cases with multiple frequencies, Strouhal number (St) corresponds to the frequency with maximum amplitude. Plots of the dominant St for different L/D over respective α ranges are presented in Fig. 14. Initiation and termination of secondary vortical shedding phase are observed to be in sync with C_{Dk}' and C_{Lk}' plots, thus verifying the precise tracing of the SI flow regime over α spectrum. It is also noticed that the magnitude of St for the primary instable state, i.e., VS flow regime, is greater than the secondary instable state, i.e., SI flow regime, which seconds the results from time history plots in terms of elongated vortical shedding period. Lower St compared to the primary instable flow regime is the characteristic property of secondary instability.

IV. CONCLUSION

A detailed numerical analysis is conducted on a system of two circular cylinders in tandem arrangement to study the impact of varying the gap ratios $L/D = 1.5$, 2, and 4 over a range of rotation rates $0 \leq \alpha \leq 15$. Different flow regimes as well as the corresponding force coefficients and their frequency spectrum for secondary vortical shedding pattern are examined to report the system behavior at varying α. Both

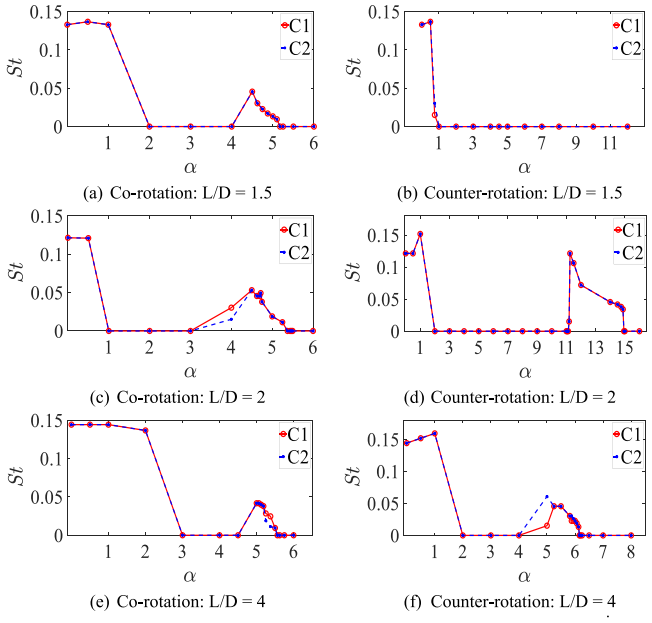

FIG. 14. Srouhal number vs α plots for $L/D = 1.5$, 2, 4 under co-rotation and counter-rotation.

co-rotation and counter-rotation of tandem cylinders are considered in this study and the corresponding flow regimes are mapped in Figs. 2 and 6, respectively, along with a comparison with a single cylinder in Fig. 2.

Based on reported literature, five distinct flow regimes have been identified for a single rotating cylinder and reported as: (1) Regime VS (Vortex Shedding), where vortices are shed from both sides of cylinder in a periodic manner; (2) Regime SW1 (Steady Wake 1), where system shows stable behavior with positive and negative shear layers shedding in elongated manner from each side of cylinder; (3) Regime SW2 (Steady Wake 2), where increased α causes shear layers from one side of cylinder to go around and extend downstream from the same side as the other shear layer; (4) Regime SI (Secondary Instability), where only one strong vortex is shed from one side of the cylinder with a large shedding time period; (5) Regime SW3 (Steady Wake 3), where shear layer wraps around the cylinder without any vortex shedding.

For co-rotating and counter-rotating tandem cylinders in the present study, different combinations of these basic flow regimes are identified. For the co-rotation configuration, both the cylinders have combined wake like a single body at all studied rotation rates, when the gap ratio is small, i.e., $L/D = 1.5$ and 2, and the wake transition is exactly the same as that of a single rotating cylinder, but, with different bounds of α. The single body behavior does not appear at $L/D = 4$ where both the cylinders have a separate wake at all the studied rotation rates. The wake transition of the downstream cylinder C2 at $L/D = 4$ is similar to that of a single cylinder with different α bounds, whereas the upstream cylinder C1 does not have a SI wake and transitions directly from SW2 to SW3 wake when SI wake of C2 disappears at the upper α boundary of the regime SW2–SI.

For the counter-rotation configuration, the single body wake appears at $L/D = 1.5$ and 2, only at low values of α when primary vortex shedding occurs (regime VS). Beyond the regime VS at $L/D = 1.5$ and 2, and regime VS–VS at $L/D = 4$, both the cylinders have individual SW1 wakes. The wake transition of each cylinder at $L/D = 4$ is the same as that of a single cylinder but with different α boundary, whereas at $L/D = 2$, only the wake transition of C1 resembles that of a single cylinder, whereas the wake of C2 transitions from SW2 to SW3 directly. The wake transition at $L/D = 1.5$ is very different from that of a single cylinder, where the SI wake does not appear at any rotation rate and the individual wake of each cylinder remains steady beyond the regime VS.

For both co-rotation and counter-rotation configurations, the mean force coefficients show a direct proportion with α. For the co-rotation configuration, both the cylinders have negative lift coefficient whereas for the counter-rotation configuration, C2 has a positive lift coefficient as it rotates in the clockwise direction. The drag coefficients exhibit repulsive and attractive forces between the cylinders for co-rotation and counter-rotation configurations, respectively. Initiation and termination of the SI wake flow for each L/D and rotation configuration are precisely traced in this study and indicated by the standard deviation of force coefficients. A significant increase in standard deviation of the force coefficients occurs when the SI wake initiates where the magnitude is the highest for the regime SI–SW3 at $L/D = 2$ for the counter-rotation configuration. Even in the regime where one cylinder has a steady wake and the other has an SI wake (i.e., regimes SW2–SI at $L/D = 4$ for co-rotation configuration and regime SI–SW3 at $L/D = 2$ for counter-rotation configuration), the standard deviation is non-zero for both the cylinders due to wake interference between both cylinders.

AUTHOR DECLARATIONS

Conflict of Interest

The authors have no conflicts to disclose.

Author Contributions

Muhammad Aneeb Siddiqui: Conceptualization (equal); Data curation (equal); Formal analysis (equal); Investigation (equal); Methodology (equal); Validation (equal); Visualization (equal); Writing – original draft (equal); Writing – review & editing (equal). **Adnan Munir:** Conceptualization (equal); Methodology (equal); Supervision (equal); Writing – review & editing (equal). **Muhammad Hamza Ali:** Formal analysis (equal); Visualization (equal); Writing – original draft (equal); Writing – review & editing (equal). **Ming Zhao:** Supervision (equal); Writing – review & editing (equal). **Penghao Duan:** Resources (equal); Writing – review & editing (equal). **Muhammad Nafees Mumtaz Qadri:** Writing – review & editing (equal).

DATA AVAILABILITY

The data that support the findings of this study are available from the corresponding authors upon reasonable request.

APPENDIX: GRID SIZE INDEPENDENCE STUDY AND VALIDATION OF THE NUMBERICAL MODEL

1. Grid size independence study

A detailed mesh sensitivity study is done by making three distinct meshes for each L/D considered in this study and the most accurate mesh, considering the computational power and numerical

TABLE I. Mesh sensitivity study for $L/D = 1.5, 2, 4$ at $\alpha = 0$ and $\alpha = 6$.

			Mesh 1		Mesh 2		Mesh 3	
			$\frac{\delta r}{D} = 0.000\,45$ $N_c = 116$ $N_t = 60\,050$		$\frac{\delta r}{D} = 0.000\,37$ $N_c = 156$ $N_t = 98\,000$		$\frac{\delta r}{D} = 0.000\,28$ $N_c = 193$ $N_t = 141\,050$	
Gap ratio L/D	Non-dimensional rotation (α)	Cylinder	$\overline{C_L}$	$\overline{C_D}$	$\overline{C_L}$	$\overline{C_D}$	$\overline{C_L}$	$\overline{C_D}$
1.5	0	C1	0.0110	1.1755	0.0109	1.1759	0.0108	1.1762
		C2	0.0329	0.0850	0.0327	0.0854	0.0324	0.0856
	6	C1	27.208	29.091	27.329	29.178	27.387	29.202
		C2	28.803	29.891	28.933	29.986	28.996	30.015
			$\frac{\delta r}{D} = 0.000\,65$ $N_c = 104$ $N_t = 50\,370$		$\frac{\delta r}{D} = 0.000\,44$ $N_c = 136$ $N_t = 90\,950$		$\frac{\delta r}{D} = 0.000\,35$ $N_c = 164$ $N_t = 130\,638$	
Gap ratio L/D	Non-dimensional rotation (α)	Cylinder	C_L	C_D	C_L	C_D	C_L	C_D
2	0	C1	0.0037	1.1460	0.0037	1.1450	0.0036	1.1450
		C2	0.0145	0.0852	0.0142	0.0837	0.0143	0.0840
	6	C1	28.740	27.610	28.770	27.705	28.877	27.705
		C2	30.741	28.514	30.816	28.371	30.913	28.601
			$\frac{\delta r}{D} = 0.000\,53$ $N_c = 112$ $N_t = 50\,137$		$\frac{\delta r}{D} = 0.000\,41$ $N_c = 156$ $N_t = 90\,800$		$\frac{\delta r}{D} = 0.000\,33$ $N_c = 176$ $N_t = 130\,045$	
Gap ratio L/D	Non-dimensional rotation (α)	Cylinder	$\overline{C_L}$	$\overline{C_D}$	$\overline{C_L}$	$\overline{C_D}$	$\overline{C_L}$	$\overline{C_D}$
4	0	C1	0.2941	1.2486	0.2956	1.2507	0.2968	1.2510
		C2	0.9448	0.6933	0.9541	0.7008	0.9575	0.7019
	6	C1	32.192	19.156	32.510	19.531	32.565	19.569
		C2	31.9922	20.1427	32.351	20.519	32.411	20.592

results, is used for further study. In the majority of cases, secondary instability subsides at around $\alpha = 6$. Two flow states, i.e., $\alpha = 0$ and $\alpha = 6$ (co-rotation), are used to compare the mesh results for each L/D as these states encapsulate the two extremes for the present study. Table I shows the mesh sensitivity study results where $\delta r/D$ is the diameter-normalized first cell height from cylinder's surface, N_c shows the number of elements at the cylinder's circumference, and N_t shows the cell count for the overall mesh. The differences between normal (Mesh 2) and fine (Mesh 3) mesh density settings are observed to be very small. Thus, the normal mesh density settings (Mesh 2) are employed for all the simulations in this study.

TABLE II. Validation study at $Re = 100$.

		Present study		(Mahír and Altaç, 2008)		(Nemati *et al.*, 2012)		Present study	(Nemati *et al.*, 2012)
Gap Ratio (L/D)	Cylinder	$\overline{C_L}$	$\overline{C_D}$	$\overline{C_L}$	$\overline{C_D}$	$\overline{C_L}$	$\overline{C_D}$	St	St
1.5	C1	0.0109	1.1759	⋯	⋯	0.01	1.23	0.1329	0.1308
	C2	0.0327	0.0854	⋯	⋯	0.01	0.061	0.1329	0.1308
2	C1	0.0037	1.1450	0.0053	1.225	⋯	⋯	0.1215	⋯
	C2	0.0142	0.0837	0.0182	0.075	⋯	⋯	0.1215	⋯
4	C1	0.295	1.2507	0.3380	1.31	⋯	⋯	0.1443	0.147
	C2	0.9541	0.7008	1.0288	0.764	⋯	⋯	0.1443	0.147

TABLE III. Validation study results at Re = 200.

Gap Ratio (L/D)	Cylinder	Present study		(Darvishyadegari and Hassanzadeh, 2019; Dehkordi *et al.*, 2011)		(Meneghini *et al.*, 2001)		(Mahír and Altaç, 2008)		Present study	(Darvishyadegari and Hassanzadeh, 2019)	(Meneghini *et al.*, 2001)	(Mahír and Altaç, 2008)
		$\overline{C_L}$	$\overline{C_D}$	$\overline{C_L}$	$\overline{C_D}$	$\overline{C_L}$	$\overline{C_D}$	$\overline{C_L}$	$\overline{C_D}$	*St*	*St*	*St*	*St*
1.5	C1	0.0150	1.0597	0.014	1.05	⋯	1.06	⋯	⋯	0.167	0.175	0.167	⋯
	C2	0.0381	0.1920	0.0424	−0.15	⋯	−0.18	⋯	⋯	0.167	0.175	0.167	⋯
2	C1	0.0195	1.0259	0.007	1.03	⋯	1.03	0.0240	1.06	0.1329	0.138	0.130	0.130
	C2	0.0847	0.1998	0.028	−0.16	⋯	−0.17	0.12	−0.21	0.1329	0.138	0.130	0.130
4	C1	0.5165	1.1979	⋯	1.16	0.7	1.18	0.4950	1.34	0.1689	0.179	0.174	0.181
	C2	1.0850	0.3699	⋯	0.52	1.5	0.38	1.2728	0.558	0.1689	0.179	0.174	0.181

2. Validation of the numerical model

Force coefficients along with Strouhal number are used to perform the model validation study. Since the numerical results for high-speed rotating tandem cylinders for different gap ratios are not vastly available, the comparison is done at $\alpha = 0$. Numerical simulations are conducted at Re = 100 and 200, and the results are presented in Tables II and III, respectively. The blank space in the table shows that the respective studies have not provided quantitative data for that specific flow condition. Decent agreement between the results of the present study and prior literature shows the reliability of the computational setup. Furthermore, this computational model is the same as that used by Ali *et al.* (2023). They conducted a detailed validation (refer to the Appendix of the said study) by presenting a comparison with numerical and experimental studies on single and multiple rotating/non-rotating cylinders, demonstrating the accuracy of the setup. Thus, the same setup is employed to perform the present numerical study.

REFERENCES

Alam, M. M., "Lift forces induced by phase lag between the vortex sheddings from two tandem bluff bodies," J. Fluids Struct. **65**, 217–237 (2016).

Ali, M. H., Munir, A., and Zhao, M., "Numerical investigation of flow across three co-rotating cylinders in side-by-side arrangement," Phys. Fluids **35**(11), 113601 (2023).

Ansari, M., Naeeni, S. T. O., and Moradi, M., "Investigating the flow and heat transfer characteristics of two co/counter-rotating circular cylinders at a low Reynolds number," Iran. J. Sci. Technol. Trans. Mech. Eng. **48**(1), 193–209 (2024).

Behara, S., Chandra, V., and Prashanth, N. R., "Three-dimensional transition in the wake of two tandem rotating cylinders," J. Fluid Mech. **951**, A29 (2022).

Bhattacharyya, S., Khan, I. H., Verma, S., Kumar, S., and Poddar, K., "Experimental investigation of three-dimensional modes in the wake of a rotationally oscillating cylinder," J. Fluid Mech. **950**, A10 (2022).

Bhattacharyya, S., Naidu S, R., Poddar, K., and Kumar, S., "Flow past a rotationally oscillating cylinder near a plane wall," Phys. Rev. Fluids **8**(9), 94102 (2023).

Carmo, B. S., Meneghini, J. R., and Sherwin, S. J., "Secondary instabilities in the flow around two circular cylinders in tandem," J. Fluid Mech. **644**, 395–431 (2010).

Chan, A. S., Dewey, P. A., Jameson, A., Liang, C., and Smits, A. J., "Vortex suppression and drag reduction in the wake of counter-rotating cylinders," J. Fluid Mech. **679**, 343–382 (2011).

Chan, A. S. and Jameson, A., "Suppression of the unsteady vortex wakes of a circular cylinder pair by a doublet-like counter-rotation," Int. J. Numer. Methods Fluids **65**, 236–253 (2010).

Chatterjee, D. and Chaitanya, N. V. V. K., "Convective transport around two rotating tandem circular cylinders at low Reynolds numbers," Sādhanā **45**(1), 107 (2020).

Chatterjee, D., Gupta, K., Kumar, V., and Varghese, S. A., "Rotation induced flow suppression around two tandem circular cylinders at low Reynolds number," Fluid Dyn. Res. **49**(4), 045503 (2017).

Darvishyadegari, M. and Hassanzadeh, R., "Heat and fluid flow around two co-rotating cylinders in tandem arrangement," Int. J. Therm. Sci. **135**, 206–220 (2019).

De Marco, A., Mancini, S., Pensa, C., Calise, G., and De Luca, F., "Flettner rotor concept for marine applications: A systematic study," Int. J. Rotating Mach. **2016**, 1 (2016).

Dehkordi, B. G., Moghaddam, H. S., and Jafari, H. H., "Numerical simulation of flow over two circular cylinders in tandem arrangement," J. Hydrodyn. **23**(1), 114–126 (2011).

Díaz, F., Gavaldà, J., Kawall, J. G., Keffer, J. F., and Giralt, F., "Vortex shedding from a spinning cylinder," Phys. Fluids **26**(12), 3454–3460 (1983).

Dubois, R. and Andrianne, T., "Flow around tandem rough cylinders: Effects of spacing and flow regimes," J. Fluids Struct. **109**, 103465 (2022).

Hosseini, N., Griffith, M. D., and Leontini, J. S., "Flow states and transitions in flow past arrays of tandem cylinders," J. Fluid Mech. **910**, A34 (2021).

Khan, I. H., Sunil, P., Bhattacharyya, S., Yadav, R., Poddar, K., and Kumar, S., "Flow past two rotationally oscillating cylinders," J. Fluid Mech. **969**, 1–41 (2023).

Kiya, M., Mochizuki, O., Ido, Y., Suzuki, T., and Arai, T., "Flip-flopping flow around two bluff bodies in tandem arrangement," in Bluff-Body Wakes, Dynamics and Instabilities (1993).

Kiya, M., Arie, M., Tamura, H., and Mori, H., "Vortex shedding from two circular cylinders in a staggered arrangement," ASME J. Fluids Eng. **102**(2), 166–171 (1980).

Krishna Chaitanya, N. V. V. and Chatterjee, D., "Influence of counter rotation on fluid flow and heat transfer around tandem circular cylinders at low Reynolds number," J. Braz. Soc. Mech. Sci. Eng. **43**(7), 357 (2021).

Kumar, S., Gonzalez, B., and Probst, O., "Flow past two rotating cylinders," Phys. Fluids **23**(1), 014102 (2011).

Li, J., Lin, H., Sun, C., Jiao, B., Sun, G., and Cao, F., "Analysis of aerodynamic performance and application of flettner rotor," J. Inst. Eng.: Ser. C **105**, 1373–1383 (2024).

Lu, L., Qin, J. M., Teng, B., and Li, Y. C., "Numerical investigations of lift suppression by feedback rotary oscillation of circular cylinder at low Reynolds number," Phys. Fluids **23**(3), 033601 (2011).

Mahír, N. and Altaç, Z., "Numerical investigation of convective heat transfer in unsteady flow past two cylinders in tandem arrangements," Int. J. Heat Fluid Flow **29**(5), 1309–1318 (2008).

Meneghini, J. R., Saltara, F., Siqueira, C. L. R., and Ferrari, J. A., Jr., "Numerical simulations of flow interference beteen two circular cylinders in tandem and side by side arrangements," J. Fluids Struct. **15**, 327–350 (2001).

Mittal, S. and Kumar, B., "Flow past a rotating cylinder," J. Fluid Mech. **476**, 303–334 (2003).
Mittal, S., Kumar, V., and Raghuvanshi, A., "Unsteady incompressible flows past two cylinders in tandem and staggered arrangements," Int. J. Numer. Methods Fluids **25**(11), 1315–1344 (1997).
Moriya, M., Alam, M. M., Takai, K., Sakamoto, H., Matsumoto, M., Shirato, H., Araki, K., Haramura, T., Hashimoto, T., Kobayashi, H., Okumura, M., Matsutani, Y., Park, C.-W., Lee, S.-J., Luo, S. C., Khoo, B. C., Tong, X. H., Ohya, Y., Watanabe, K., Li, Y. F., Flay, R. G. J., and Richards, P. J., "Fluctuating fluid forces acting on two circular cylinders in a tandem arrangement at a subcritical Reynolds Number," J. Wind Eng., JAWE **2001**(89), 697–724.
Munir, A., Zhao, M., Wu, H., and Lu, L., "Numerical investigation of wake flow regimes behind a high-speed rotating circular cylinder in steady flow," J. Fluid Mech. **878**, 875–906 (2019).
Nemati, H., Farhadi, M., Sedighi, K., Pirouz, M. M., and Abatari, N. N., "Convective heat transfer from two rotating circular cylinders in tandem arrangement by using lattice Boltzmann method," Appl. Math. Mech. **33**(4), 427–444 (2012).
Pal Singh Bhinder, A., Sarkar, S., and Dalal, A., "Flow over and forced convection heat transfer around a semi-circular cylinder at incidence," Int. J. Heat Mass Transfer **55**(19–20), 5171–5184 (2012).
Rastan, M. R., Sohankar, A., and Alam, M. M., "Flow and heat transfer across two inline rotating cylinders: Effects of blockage, gap spacing, Reynolds number, and rotation direction," Int. J. Heat Mass Transfer **174**, 121324 (2021).
Seddiek, I. S. and Ammar, N. R., "Harnessing wind energy on merchant ships: Case study Flettner rotors onboard bulk carriers," Environ. Sci. Pollut. Res. **28**(25), 32695–32707 (2021).
da Silva, A. R. and de Lima, A. M. G., "Analysis of flow dynamics around two rotating circular cylinders in tandem and side by side," Int. J. Adv. Eng. Res. Sci. **7**(6), 366–379 (2020).
Stojković, D., Breuer, M., and Durst, F., "Effect of high rotation rates on the laminar flow around a circular cylinder," Phys. Fluids **14**(9), 3160–3178 (2002).
Wu, Z., Fundamentals of Pulverised Coal Combustion (IEA Clean Coal Centre, 2005). https://www.sustainable-carbon.org/wp-content/uploads/dlm_uploads/reports/Combustion/fundamentals-of-pulverised-coal-combustion-ccc-95.pdf
Yang, Y., Wang, C., Guo, R., and Zhang, M., "Numerical analyses of the flow past a short rotating cylinder," J. Fluid Mech. **975**, 1–35 (2023).
Yoon, H. S., Kim, J. H., Chun, H. H., and Choi, H. J., "Laminar flow past two rotating circular cylinders in a side-by-side arrangement," Phys. Fluids **19**(12), 1–5 (2007).
Zdravkovich, M. M., "REVIEW-Review of flow interference between two circular cylinders in various arrangements," ASME J. Fluids Eng. **99**(4), 618–633 (1977).
Zdravkovich, M. M., "The effects of interference between circular cylinders in cross flow," J. Fluids Struct. **1**(2), 239–261 (1987).
Zhang, C., Tang, G., Lu, L., Jin, Y., An, H., and Cheng, L., "Flow-induced vibration of two tandem square cylinders at low Reynolds number: Transitions among vortex-induced vibration, biased oscillation and galloping," J. Fluid Mech. **986**, 1–38 (2024).